

Near-field amplitude and phase recovery using phase-shifting interferometry

B. Deutsch[†], R. Hillenbrand^{††}, and L. Novotny^{†*}

[†] *The Institute of Optics, University of Rochester, Rochester, NY 14611*

^{††} *Nano-Photonics Group, Max-Planck-Institut für Biochemie, D-82152 Martinsried, Germany*

** novotny@optics.rochester.edu*

** www.nano-optics.org*

Abstract: Scattering-type scanning near-field optical microscopy has allowed for investigation of light-matter interaction of a large variety of samples with excellent spatial resolution. Light incident on a metallic probe experiences an amplitude and phase change on scattering, which is dependent on optical sample properties. We implement phase-shifting interferometry to extract amplitude and phase information from an interferometric near-field scattering system, and compare recorded optical images with theoretical predictions. The results demonstrate our ability to measure, with nanoscale resolution, amplitude and phase distributions of optical fields on sample surfaces. The here-introduced phase-shifting method is considerably simpler than heterodyne methods and less sensitive to errors than the two-step homodyne method.

© 2008 Optical Society of America

OCIS codes: (180.4243) Near-field microscopy; (180.5810) Scanning microscopy; (120.3180) Interferometry; (120.5050) Phase measurement.

References and links

1. A. Cvitkovic, N. Ocelic, and R. Hillenbrand, "Analytical model for quantitative prediction of material contrasts in scattering-type near-field optical microscopy," *Opt. Express* **15**, 8550–8565 (2007).
2. R. Hillenbrand and F. Keilmann, "Material-specific mapping of metal/semiconductor/dielectric nanosystems at 10 nm resolution by back-scattering near-field optical microscopy," *Appl. Phys. Lett.* **80**, 25 (2002).
3. R. Hillenbrand and F. Keilmann, "Complex optical constants on a subwavelength scale," *Phys. Rev. Lett.* **85**, 3029–3032 (2000).
4. J. E. Hall, G. P. Wiederrecht, S. K. Gray, S.-H. Chang, S. Jeon, J. A. Rogers, R. Bachelot, and P. Royer, "Heterodyne apertureless near-field scanning optical microscopy on periodic gold nanowells," *Opt. Exp.* **15**, 4098–4105 (2007).
5. N. Ocelic, A. Huber, and R. Hillenbrand, "Pseudoheterodyne detection for background-free near-field spectroscopy," *Appl. Phys. Lett.* **89**, 101124–1 (2006).
6. F. Keilmann and R. Hillenbrand, "Near-field microscopy by elastic light scattering from a tip," *Phil. Trans. R. Soc. Lond. A* **362**, 787–805 (2004).
7. L. Novotny, B. Hecht, and D. Pohl, "Implications of high resolution to near-field optical microscopy," *Ultramicroscopy* **71**, 341–344 (1998).
8. L. Novotny and S. Stranick, "Near-field optical microscopy and spectroscopy with pointed probes," *Annu. Rev. Phys. Chem.* **57**, 303–331 (2006).
9. I. Stefanon, S. Blaize, A. Bruyant, S. Aubert, G. Lerondel, R. Bachelot, and P. Royer, "Heterodyne detection of guided waves using a scattering-type scanning near-field optical microscope," *Opt. Exp.* **13**, 5553–5564 (2005).
10. R. Hillenbrand, F. Keilmann, P. Hanarp, D. Sutherland, and J. Aizpura, "Coherent imaging of nanoscale plasmon patterns with a carbon nanotube optical probe," *Appl. Phys. Lett.* **83**, 368–370 (2003).
11. G. Wiederrecht, "Near-field optical imaging of noble metal nanoparticles," *Eur. Phys. J. Appl. Phys.* **28**, 3–18 (2004).

12. G. Wurtz, R. Bachelot, and P. Royer, "Imaging a GaAlAs laser diode in operation using apertureless scanning near-field optical microscopy," *Eur. Phys. J.: Appl. Phys.* **5**, 269–275 (1999).
13. M. Labardi, S. Patanè, and M. Allegrini, "Artifact-free near-field optical imaging by apertureless microscopy," *Appl. Phys. Lett.* **77**, 621–623 (2000).
14. B. Knoll and F. Keilmann, "Enhanced dielectric contrast in scattering-type scanning near-field optical microscopy," *Opt. Commun.* **182**, 321–328 (2000).
15. T. Taubner, R. Hillenbrand, and F. Keilmann, "Performance of visible and mid-infrared scattering-type near-field optical microscopes," *J. Microsc.* **210**, 311–314 (2003).
16. R. Hillenbrand, B. Knoll, and F. Keilmann, "Pure optical contrast in scattering-type scanning near-field microscopy," *J. Microsc.* **202**, 77–83 (2001).
17. J. Bruning, D. Herriott, J. Gallagher, D. Rosenfeld, A. White, and D. Brangaccio, "Digital wavefront measuring interferometer for testing optical surfaces and lenses," *Appl. Opt.* **13**, 2693–2703 (1974).
18. J. Greivenkamp and J. Bruning, "Phase-shifting interferometers," in *Optical Shop Testing*, D. Malacara, ed., pp. 501–598 (Wiley, NY, 1991).
19. Y. Surrel, "Phase stepping: a new self-calibrating algorithm," *Appl. Opt.* **32**, 3598–3600 (1993).
20. P. S. Carney, R. A. Frazin, S. I. Bozhevolnyi, V. S. Volkov, A. Boltasseva, and J. C. Schotland, "Computational Lens for the Near Field," *Phys. Rev. Lett.* **92**, 163903 (2004).
21. J. Sun, J. Schotland, and P. S. Carney, "Strong probe effects in near-field optics," *J. Appl. Phys.* (2007 (in press)).
22. L. Novotny and B. Hecht, *Principles of Nano Optics* (Cambridge University Press, New York, 2006).
23. A. Huber, N. Ocelic, D. Kazantsev, and R. Hillenbrand, "Near-field imaging of mid-infrared surface phonon polariton propagation," *Appl. Phys. Lett.* **87**, 081103 (2000).
24. A. Bouhelier, M. Beversluis, A. Hartschuh, and L. Novotny, "Near-field second-harmonic generation induced by local field enhancement," *Phys. Rev. Lett.* **90**, 013903 (2003).
25. D. Phillion, "General methods for generating phase-shifting interferometry algorithms," *Appl. Opt.* **36**, 8098–8115 (1997).

1. Introduction

Scattering-type scanning near-field optical microscopy (sSNOM) combines the resolution of atomic force microscopy with the chemical sensitivity of optical spectroscopy. It has been shown that information about the local optical field can be used to determine the distribution of a sample's complex-valued dielectric function with spatial resolution of a few tens of nanometers[1, 2, 3]. Various configurations of sSNOM have been implemented recently[4, 5, 6]. Most commonly, a sharp metal tip is brought within close proximity to a sample surface, and the tip-sample region is illuminated with an external laser beam, creating a region of enhanced electric near field[7, 8]. Light experiences a change in amplitude and phase relative to the incident light upon scattering from this region, and the amplitude and phase change depend on the local dielectric properties of the sample and the local optical field illuminating the tip. The collected light can be composed of the incident field plus propagating fields close to the sample[9], evanescent fields[10], or a combination of both[11]. There is interest in measuring the amplitude and phase changes separately, since these signals contain different but complimentary information about the sample. In sSNOM, the tip is raster-scanned over the sample surface in close proximity and for each image pixel the optical phase and amplitude is recorded, usually interferometrically using lock-in techniques[6].

While the concept of sSNOM is well-established, the widespread use of the method is still challenged by basic issues. For example, the collected signal is typically weak, and often competes with strong background radiation resulting from stray light and scattering from regions other than the near-field of the sample. This requires the background to be suppressed during measurement, and various approaches have been introduced with this aim.

One method of background suppression involves the modulation of the tip-sample separation, which is usually accomplished by vibrating an AFM cantilever at its resonance. This creates an optical modulation of the collected light, which is then demodulated at higher harmonics of the tip vibration frequency[12, 13, 14, 3]. This has the effect of filtering out background radiation, leaving predominantly light scattered from the near-field region of the sample. The tip modulation technique may be combined with homodyne[15] or heterodyne[3] interferometry.

The latter makes it possible to simultaneously recover amplitude and phase of the scattered light[16, 15]. Another method for recovery of this information is pseudoheterodyning, in which a small modulation of the reference beam is introduced, along with demodulation techniques similar to heterodyning[5]. Heterodyne and pseudoheterodyne sSNOM have been applied to a variety of problems, including nondestructing mapping of complex dielectric properties, and mapping complex fields in nanophotonic structures[6].

Two-step homodyning is another method of amplitude and phase extraction, in which two homodyned interferometric measurements are taken at each pixel, separated by $\pi/2$ radians in optical phase, typically accomplished by movement of the reference mirror[15]. From these two measurements, amplitude and phase may be extracted in post-processing. The two measurements may be instantaneous or may be integrated over arbitrarily long times, and they are usually time-multiplexed.

These three methods suffer from general interferometric detection difficulties, as well as technique-specific problems. Heterodyning is complicated due to the necessity of an additional collinear, frequency shifted reference beam (usually generated by acousto-optic modulators). Both heterodyne and pseudoheterodyne methods require the generation of a phase-locked reference signal at sidebands of harmonics of the modulation frequency. Two-step homodyning is slow due to the necessity of driving the reference piezo with a square waveform, and is prone to errors associated with an instantaneous measurement. Finally, all three methods are subject to common problems associated with interferometric detection, including sensitivity to detector nonlinearities, vibration and atmospheric turbulence, and laser amplitude fluctuations.

We present an alternative method of amplitude and phase recovery for sSNOM, drawing from the field of phase-shifting interferometry (PSI), which has been used for several decades in optical testing, and which has the potential to mitigate these issues[17]. In PSI, the reference mirror is moved through at least three phase steps, which are usually equally spaced. Interferometric optical measurements at each of these steps are used to solve for amplitude and phase, and the constant noninterferometric signal is eliminated. This method exhibits the relative simplicity of the pseudo-heterodyne method while reducing the uncertainty[18] in the two-step homodyne process and maintaining reasonable scan speeds. Furthermore, extensive work has already been published on suppression of common interferometric errors, which may plausibly be applied to SNOM applications.

2. Phase shifting interferometry

The signal at the detection plane of a basic interferometer is described by

$$I = I_s + I_r + \sqrt{I_s I_r} \cos(\phi + \delta_n + \Delta), \quad (1)$$

where I_s is the signal intensity, I_r is the reference beam intensity, ϕ is the phase change on scattering, and δ_n is the phase added by reference mirror movement. It is understood that I_s and ϕ are functions of the location (x, y) on the sample, i.e. each image pixel gives rise to a different I_s and ϕ . Δ is a constant phase offset due to the relative lengths of the two arms of the interferometer, but it may be arbitrarily set to zero if we are only interested in the relative phase at different sample locations. Equation 1 may be rewritten as

$$I = A + R \cos(\phi + \delta_n). \quad (2)$$

Here, A is an offset term, and R represents a coefficient proportional to the scattered amplitude. If there are N equal phase steps (with index n) associated with the mirror movement, we can write

$$\delta_n = \frac{2\pi n}{N}. \quad (3)$$

In PSI, at least three optical measurements are taken for each pixel (x, y) at different values of δ_n , so equation 2 yields a system of at least three equations and exactly three unknown quantities: A , R and ϕ . Following the work of Bruning, et al., ϕ can be calculated using the N-bin algorithm[17], in which

$$\tan(\phi) = -\frac{\sum_{n=0}^{N-1} I(n) \sin\left(\frac{2\pi n}{N}\right)}{\sum_{n=0}^{N-1} I(n) \cos\left(\frac{2\pi n}{N}\right)}. \quad (4)$$

While the optical testing community is not generally interested in the value of R , it is straightforward to show by a similar derivation that

$$R = \left(\left(\sum_{n=0}^{N-1} I(n) \sin\left(\frac{2\pi n}{N}\right) \right)^2 + \left(\sum_{n=0}^{N-1} I(n) \cos\left(\frac{2\pi n}{N}\right) \right)^2 \right)^{1/2}. \quad (5)$$

Surrell et al. point out that the phase calculation resulting from the N-bin algorithm is sensitive to linear miscalibrations of the piezo which is responsible for the phase steps.[19] To understand the error associated with miscalibration we rewrite the interferometric signal in equation 2 as

$$I(n) = A + R \cos\left(\phi + 2\pi(1 + \varepsilon)\frac{n}{N}\right). \quad (6)$$

where ε is the percent linear miscalibration. Higher order miscalibrations are also possible, but their effect is generally much smaller. The phase error is then derived to be

$$\Delta\phi = \frac{N-1}{N} \pi\varepsilon - \frac{\pi\varepsilon}{N \sin\left(\frac{2\pi}{N}\right)} \sin\left(2\phi - \frac{2\pi}{N}\right), \quad (7)$$

where we note that in the limit of large N we come to a minimum error value of

$$\Delta\phi_{min} = \pi\varepsilon - \frac{\varepsilon}{2} \sin(2\phi), \quad (8)$$

which, besides a constant phase offset, yields a dependence on the actual phase. Surell et al. propose an $(N+1)$ -bin algorithm, in which the phase is calculated as

$$\tan(\phi) = \frac{\frac{I(0)-I(N)}{2} \cot\left(\frac{2\pi}{N}\right) - \sum_{n=1}^{N-1} I(n) \sin\left(\frac{2\pi n}{N}\right)}{\frac{I(0)+I(N)}{2} + \sum_{n=1}^{N-1} I(n) \cos\left(\frac{2\pi n}{N}\right)}, \quad (9)$$

and the error is shown to be

$$\Delta\phi_{min} \approx \pi\varepsilon + \left(\frac{\pi\varepsilon}{N \sin\left(\frac{2\pi}{N}\right)} \right)^2 \sin(2\phi), \quad (10)$$

yielding a much smaller minimum phase dependence of

$$\Delta\phi_{min} \approx \pi\varepsilon + \left(\frac{\varepsilon}{2} \right)^2 \sin(2\phi), \quad (11)$$

in the limit of large N .

In the limiting case of two phase steps separated by $\pi/2$, the here-outlined approach is analogous to two-step homodyning. In this case, since homodyning forces the optical signal A in equation 2 to be equal to zero, only two equations are required at minimum to solve for R and ϕ . However, with many phase steps redundant measurements are acquired almost simultaneously, and these can be used to drastically decrease the uncertainty of the measurement, and render it insensitive to linear piezo miscalibration.

3. Phase-shifting interferometry applied to near-field microscopy

We have developed a scattering-based near-field optical microscope (sSNOM) and implemented phase-shifting interferometry (PSI) for local amplitude and phase extraction. The instrument was applied to study fields scattered by polystyrene spheres on glass. The experimental setup is illustrated in Fig. 1. A diode laser with wavelength 831nm is used as the source in a Michelson interferometer. Balanced photodetection is used, in which a portion of the source beam is sampled and subtracted from the measured signal. This decreases effects due to power fluctuations, and helps to utilize the full dynamic range of the detector. The sample is illuminated via a parabolic mirror ($N.A. \approx 1/2$), and the near-field probe consists of a Pt-coated AFM tip, vibrated at its resonance frequency of 150kHz with an amplitude of approximately 10nm. The sample is raster scanned below the tip and a tapping-mode-like feedback mechanism maintains a constant probe-sample separation. A sinusoidal signal is sent to the reference mirror piezo, moving it through a 2π phase shift at least once for each pixel. The detector signal is sent to a lock-in amplifier, which demodulates the signal at twice the resonance frequency of the AFM cantilever. The lock-in output is recorded simultaneously with the sinusoidal reference-mirror signal and sample height for each pixel. In post-processing, the lock-in output at the time of each of 200 equal phase steps is extracted for each pixel, and equations 5 and 9 are used respectively to calculate amplitude and phase of the demodulated signal.

The demodulation process somewhat complicates the interpretation of the recorded signal by adding a term that is proportional to the product of the reference and signal amplitudes [16]. This term does not change with the reference phase, however, so it is eliminated by the PSI algorithm.

PSI-SNOM was used to scan 356nm diameter polystyrene spheres on glass, and the resulting topography, amplitude and phase images are illustrated in 2. A ring-like amplitude modulation pattern is evident, with an area of high amplitude next to the bead, opposite the direction of incident radiation. This area corresponds to a dip in the phase of approximately 30 degrees.

To compare the measurements with theoretical predictions we consider the scattered field as a series of interaction orders [20, 21]

$$\mathbf{E}_{\text{scatt}} = \mathbf{E}_T + \mathbf{E}_{ST} + \mathbf{E}_{TS} + \mathbf{E}_{TST} + \dots \quad (12)$$

Here, \mathbf{E}_T corresponds to the incident field scattered by the tip, \mathbf{E}_{ST} to the field scattered by the sample and then by the tip, \mathbf{E}_{TS} to the field scattered by the tip and then by the sample, and \mathbf{E}_{TST} to the field scattered by the tip then the sample and finally the tip again. In Eq. (12) we have assumed that the sample is weakly scattering and have rejected the term \mathbf{E}_S because it is rejected by the tip-modulation technique and detection at higher harmonics [15].

In our configuration, \mathbf{E}_T is proportional to the incident field evaluated at the location of the tip, i.e. $\mathbf{E}_o(\mathbf{r}_o)$, whereas \mathbf{E}_{ST} is proportional to the field scattered by the sphere located at \mathbf{r} and evaluated at the location of the tip, i. e. $\mathbf{E}_{\text{sphere}}(\mathbf{r}_o, \mathbf{r})$. The polarizability of the tip, $\vec{\alpha}_T$ is the proportionality constant in both cases. \mathbf{E}_{ST} is evaluated by a full Mie scattering solution [22]. By reciprocity, \mathbf{E}_{TS} is equal to \mathbf{E}_{ST} [21]. In our experiments we keep the position of the tip fixed

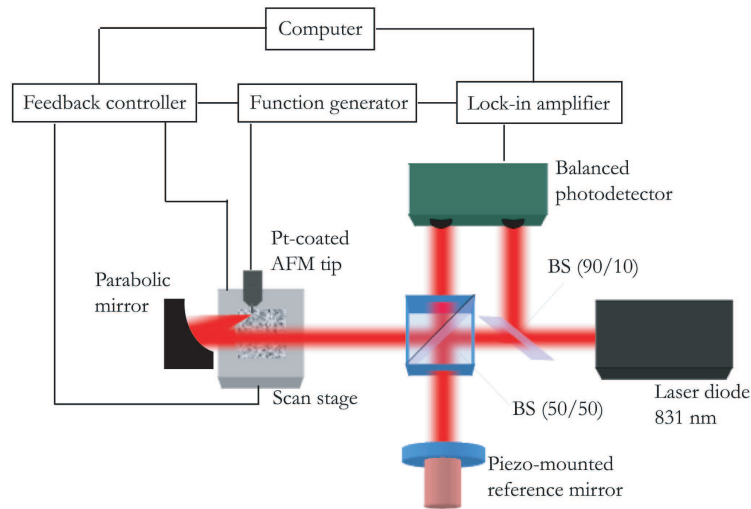


Fig. 1. Schematic of the sSNOM setup. Light scattered from the tip is collected by a Michelson interferometer with a piezo-mounted reference mirror. The light is collected by a balanced photodetector and demodulated by a lock-in amplifier.

and raster-scan the sample in the (x,y) plane. Thus, the image coordinates correspond to those of the sphere location $\mathbf{r} = (x,y,z=0)$. We assume plane-wave illumination, which is a good approximation considering the low N.A. illumination and the size of the tip and scan region. Higher N.A. illumination would complicate the scattering terms beginning with S, but leave the T terms nearly unchanged. Neglecting higher order terms in Eq. (12) and assuming a field that slowly varies in the z -direction, we can write the detected signal as[23]

$$\text{signal}(x,y) \propto [\mathbf{E}_0 + 2\mathbf{E}_{\text{sphere}}(x,y)] \cdot \mathbf{n}_z, \quad (13)$$

where \mathbf{n}_z is the unit vector in direction of the tip axis. The field components perpendicular to the tip axis can be ignored because $\vec{\alpha}_T$ for a metal tip is much stronger along its axis than transverse to it [24]. Furthermore, the polarization of the reference beam is aligned along the tip axis.

Fig. 3 shows the calculated amplitude and phase distribution for the field near a polystyrene sphere according to Eq. (13). The amplitude distribution exhibits a characteristically high scattering amplitude in the shadow of the sphere, as well as fringes on the irradiated side originating from the interference of \mathbf{E}_0 and $\mathbf{E}_{\text{sphere}}$. These features agree very well with the experimental image shown previously in Fig. 2. Similar agreement is obtained for the phase distribution, which varies in the range of $\Phi = [0..27]$ degrees. We conclude that phase-shifting-interferometry in combination with scattering-based near-field microscopy provides measurements of the complex local field distribution near a sample surface. The number of terms in Eq. (12) that need to be retained depends on the properties of the sample. It can be expected that for a sample with resonant metal structures or significant periodicity the \mathbf{E}_{TST} term will become important. We would like to emphasize that the recorded amplitude and field distribu-

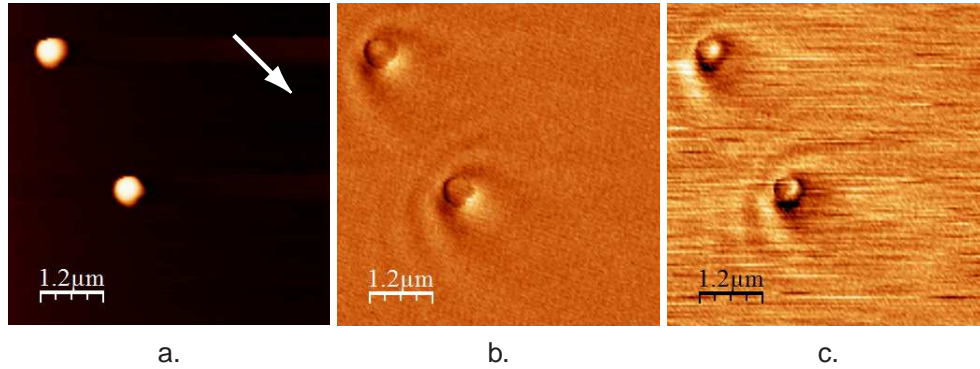


Fig. 2. (a) Topography, (b) demodulated optical amplitude, and (c) demodulated optical phase of laser-irradiated polystyrene spheres on glass. The white arrow represents the in-plane projection of the incident wave vector.

tions together with the topology are sufficient for a reconstruction of the spatial distribution of the dielectric function, $\epsilon(\mathbf{r})$, of an object supported by the substrate[20]. In order to obtain the full angular spectrum of the sample, additional degrees of freedom would be needed, e.g. spectroscopic information or variability of the illumination angle. Studies in this direction are in progress in our laboratory.

4. Sources of error

One advantage of PSI is that decades of research have been devoted to its development, including characterizing and overcoming inherent errors. If phase and amplitude information is to be used to extract quantitative information about a sample, it is important to be able to minimize these errors. PSI-SNOM allows for significant freedom in the number of phase steps taken, the spacing between phase steps, and the algorithms for phase and amplitude extraction, including the weighting of samples and software correction through system characterization. Phillion described constraints for developing phase-shifting algorithms in order to generate results that are insensitive to detector nonlinearities, certain orders of laser fluctuation, or certain orders of piezo miscalibration[25].

Since PSI-SNOM relies heavily on post-processing, it is essential to synchronize the optical and mirror voltage data sets. In the case of a homodyned signal, the lock-in process adds an electronic delay to the optical signal, and the mirror voltage signal will thus have to be artificially delayed in post-processing. This is a static characteristic of the system, however, and once it is calibrated, no further adjustment is required.

5. Conclusion

PSI-SNOM exhibits several advantages over other sSNOM methods for amplitude and phase recovery. There is no need for a frequency-shifted reference beam as in heterodyne methods, or for a phase-locked reference signal at sidebands of the modulation frequency, as in heterodyne and pseudoheterodyne methods. In addition, it is more robust to sources of error than the two-step homodyne method, and indeed the flexibility of the phase-recovery algorithm makes further error optimization plausible. We have demonstrated the application of this method by obtaining demodulated amplitude and phase images of fields near polystyrene beads on glass and comparing them to a theoretical model. Application of methods from the developed field of phase-shifting interferometry should lead to reliable quantitative sample characterization with

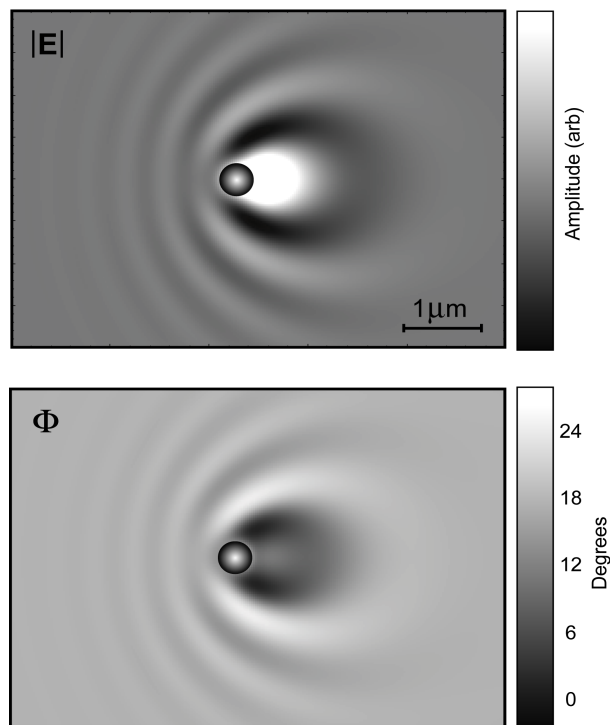


Fig. 3. Simulation of measured signal from polystyrene spheres. Amplitude and phase distributions are in good agreement with the experimental results in Fig. 2.

good spatial resolution, and we expect that with further optimization, PSI-SNOM could lead to an improvement in amplitude and phase recovery over heterodyne or pseudo-heterodyne SNOM.

Acknowledgements

The authors thank P. Scott Carney, Jin Sun and Fritz Keilmann for valuable input to this work. This work was financially supported by the Air Force Office of Scientific Research (F-49620-03-1-0379, MURI) and by the Petroleum Research Foundation (PRF 42545-AC10). R.H. was supported by BMBF grant no. 03N8705.